Results in Engineering 25 (2025) 103949

Contents lists available at ScienceDirect

Results in Engineering

journal homepage: www.sciencedirect.com/journal/results-in-engineering

Research paper

Performance evaluation of a nearest level control-based TCHB multilevel inverter for PMSM motors in electric vehicle systems

Md Showkot Hossain [a,b], Nurul Ain Mohd Said [a,b,*], Md Akib Hasan [c], Wahidah Abd Halim [a,b], Wan Noraishah Wan Abdul Munim [d], Auzani Jidin [a,b]

[a] Faculty of Electrical Technology and Engineering, Universiti Teknikal Malaysia Melaka, Melaka, Malaysia
[b] Power Electronics and Drive Research Group, Universiti Teknikal Malaysia Melaka, Melaka, Malaysia
[c] Faculty of Electrical Engineering & Technology, Universiti Malaysia Perlis, Perlis, Malaysia
[d] School of Electrical Engineering, College of Engineering, Universiti Teknologi MARA, Selangor, Malaysia

ARTICLE INFO

Keywords:
Electric vehicle
Field-oriented control
Nearest level control
Permanent magnet synchronous motor
Transistor clamped H-bridge MLI

ABSTRACT

Transistor Clamped H-Bridge (TCHB) multilevel inverter (MLI) is receiving considerable research interest because it can provide excellent outputs with a reduced number of switches and DC voltage sources compared to traditional MLI topologies. This study investigates the application of a nearest level control (NLC) technique in a three-phase TCHB inverter fed permanent magnet synchronous motor (PMSM) with a focus on improving power quality and minimizing total harmonic distortion (THD). The proposed system is modeled in MATLAB/Simulink, incorporating a field-oriented control (FOC) strategy with a proportional-integral (PI) controller for precise speed regulation of the PMSM. The NLC technique is selected for its ability to reduce switching losses and improve inverter efficiency. Key performance metrics, including THD, efficiency, and dynamic response, are analyzed under various operating conditions. Results indicate that the NLC technique reduces THD to 4.73 %, achieving smoother output waveforms and enhanced power quality. Additionally, the system demonstrates over 97 % efficiency, reliable dynamic performance, and accurate reference speed tracking during real-life driving cycle testing. These findings highlight the potential of the NLC-based TCHB inverter as a robust solution for high-performance motor drives in electric vehicle (EV) applications.

1. Introduction

Multilevel inverters play a crucial part in modern power electronics, offering advantages such as minimized harmonic distortion, decreased electromagnetic interference, and enhanced efficiency [1–5]. Among various MLI topologies, TCHB inverter is preferred because it can generate high-quality output using fewer switches and DC voltage sources [6,7]. This makes the TCHB inverter more suitable for applications like renewable energy systems and EVs that value affordability and space [8]. Despite the advantages of TCHB MLIs, one of the major challenges remains the effective control of the inverter to minimize total harmonic distortion and enhance overall system efficiency [9,10].

The performance of MLIs heavily depends on the modulation technique used, as it influences the harmonics of current and voltage within the system [11,12]. Some commonly used modulation techniques are Pulse Width Modulation (PWM), Space Vector Modulation (SVM), and Selective Harmonic Elimination (SHE) [13,14]. Although PWM and SVM are capable of generating high-quality output, they experience substantial switching losses. However, the SHE method effectively removes low-order harmonics but requires complex computations [7,14].

The NLC technique offers a direct and advantageous option, especially for MLIs at higher levels. The NLC system minimizes switching losses and improves efficiency through comparison of the reference voltage with the available voltage levels and selecting the nearest one [15,16]. The NLC method is applied and assessed in a MLI featuring an asymmetrical cascaded H-bridges (A-CHB) setup [17]. Even in the absence of filters, the results show a substantial reduction in THD. Additionally, NLC method considerably minimizes switching losses at higher levels [18]. The NLC technique was utilized in a 27-level A-CHB inverter, as demonstrated in [19], where the results indicated that the NLC method achieved the staircase output voltage with the lowest THD of approximately 3 %. This approach has demonstrated encouraging outcomes in decreasing THD and enhancing power quality [20,21].

* Corresponding author.
E-mail address: nurulain@utem.edu.my (N.A.M. Said).

https://doi.org/10.1016/j.rineng.2025.103949
Received 18 November 2024; Received in revised form 8 December 2024; Accepted 3 January 2025
Available online 3 January 2025
2590-1230/

Understanding inverter losses and efficiency is crucial for designing robust and cost-effective systems [1]. The primary causes of inverter losses are conduction and switching losses, which have a direct effect on the overall efficiency and thermal management requirements [22]. Accurate loss models, which rely on the datasheet specifications for operational devices, are crucial for conducting realistic loss analysis.

The cascaded H-bridge (CHB) inverter has been extensively investigated through academic research due to its highly modular and resilient design, which makes it a popular selection for EV applications [23,24]. Fig. 1 represents the basic schematics of an EV car system, detailing the interaction between key components such as the power source, inverter, motor, and control unit. This provides a clear representation of the system's architecture, emphasizing the role of the TCHB MLI in driving the PMSM motor. In the context of EVs, the TCHB inverter's efficiency and reliability are paramount. The TCHB topology, with its fewer switches, offers a viable solution for high-performance motor drive applications [9,25]. Previous research has demonstrated the efficacy of TCHB inverters in various applications, but their specific application in EVs, particularly with a PMSM drive, has not been extensively investigated [8,26]. This work investigates a three-phase TCHB inverter driven PMSM system, as a part of the continuing study on developing novel DC/AC inverter designs for EVs.

PMSMs are gaining popularity in the use of light-duty EV applications. They are rapidly replacing DC and induction motors in the field of variable speed drives [27]. Their high-power density, significant low-speed torque, and enhanced overall efficiency are responsible for these characteristics [28,29]. Recent studies, in reference [30], have conducted thorough comparisons of PMSMs with different rotor configurations for EVs using Finite Element (FE) analysis. To achieve the best performance in EVs, it is essential to give preference to smooth starting and operations, as well as effective usage of the direct current (DC) bus voltage. As a result, there has been a significant amount of scientific research conducted on PMSMs and their control methods [31,32]. FOC is a widely adopted control method for PMSM drives [33,34]. It is a closed-loop control method that offers excellent dynamic performance by decoupling torque and flux control. This technique has been extensively studied and documented in references [35–37]. Various methodologies for designing controllers for FOC drives were introduced in references [38] and [39].

The PI controllers were employed for both the speed controller and the current controllers. This control strategy ensures smooth starting, efficient operation, and efficient performance over a wider speed range [40].

The primary contribution of this research lies in the development and implementation of an NLC technique for a three-phase TCHB multilevel inverter. This approach addresses key challenges in reducing THD and enhancing the efficiency of the inverter for EV applications. Compared to conventional modulation methods such as PWM and SVM, the proposed NLC technique offers significant improvements in power quality and switching losses. While previous studies have explored different modulation techniques and inverter topologies, there is limited research specifically focused on the application of NLC for TCHB inverters with PMSM, particularly in EV systems. The integration of FOC with NLC in this work further enhances the precision of speed control in the PMSM, addressing performance issues related to torque ripple and energy efficiency.

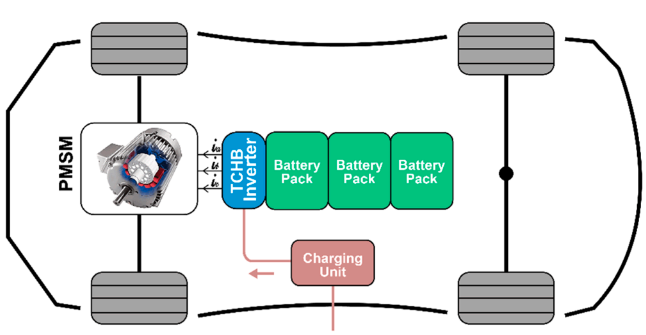

Fig. 1. Basic schematics of EV cars with inverter.

Furthermore, the use of the TCHB topology in EV applications, especially in combination with PMSM drives, represents a relatively underexplored area with significant potential [41]. This study's primary contributions include the evaluation of THD, efficiency, and dynamic response under different operational conditions for a TCHB inverter-driven PMSM system using NLC. Comprehensive simulations in MATLAB/Simulink offer insights into system behavior and potential real-world applicability. By demonstrating superior performance in terms of power quality and system stability, this research positions the NLC-based TCHB inverter as a promising approach for EV applications and renewable energy integration. The remainder of this article is structured as follows: Section 2 presents the proposed topology design, including the design of the NLC-based TCHB inverter and its performance analysis. Section 3 discusses the modeling of the PMSM and proposed controller, followed by the Verification of Inverter System Using FOC strategies for PMSM and comparison with relevant literature in Section 4. Conclusions and future research directions are outlined in Section 5.

2. Proposed multilevel inverter and its modulation strategy

2.1. TCHB multilevel inverter

The configuration of a 13-level TCHB-based cascaded multilevel inverter is shown in Fig. 2. This inverter configuration utilizes three TCHB cells and three independent DC voltage sources to generate a high-quality output with a maximum of thirteen levels. To maintain consistent increases in voltage, it is assumed that the DC voltage sources have the same magnitudes, and significant capacitances (e.g., 2200 μF) are used at the DC link.

Each TCHB inverter unit contains with a bidirectional switch made up of four diodes and one transistor. This switch is added to a standard H-bridge inverter to enhance its functionality. The bidirectional switch offers the advantage of allowing current to flow in both directions, therefore enabling the creation of five different voltage output levels: 0, $\pm 1/2V_{dc}$, and $\pm V_{dc}$ using a single TCHB inverter unit. The power switches and diodes in this topology encounter distinct standing voltages. For example, the four switches in the H-bridge ($S_{i1} - S_{i4}$) all have a constant voltage equal to V_{dc}. The idle voltage for every component of the bidirectional switch, including diodes and switch S_{i5} is equal to $\pm 1/2V_{dc}$ for balance capacitor voltage conditions.

Table 1 presents a comprehensive overview of the five operational modes available for a single TCHB inverter cell. When S_{i5} and either S_{i2} or S_{i4}, are switched appropriately, half of the output voltages are produced; number of TCHB cells is indicated by the letter 'i'. Total output voltage (V_{inv}) for a cascade of TCHB cells can be written as follows:

$$v_{inv} = v_1 + v_2 + v_3 + \ldots + v_i \quad (1)$$

In general, the topology produces $4i + 1$ output levels (where i denotes the amount of TCHB cells). By considering symmetry, a TCHB inverter with identical voltage sources (v_{dc}) and three units connected in series configuration could generate 13-level output voltage (0, $\pm\frac{1}{2}v_{dc}$, $\pm v_{dc}$, $\pm 1\frac{1}{2}v_{dc}$, $\pm 2v_{dc}$, $\pm 2\frac{1}{2}v_{dc}$, $\pm 3v_{dc}$).

2.2. Nearest level control technique

For multilevel inverters, a simple yet efficient strategy is the NLC methodology [40]. This system works by comparing the reference voltage to all of voltage levels that are available, then choose the voltage level the one nearest to the reference. This method generates gating

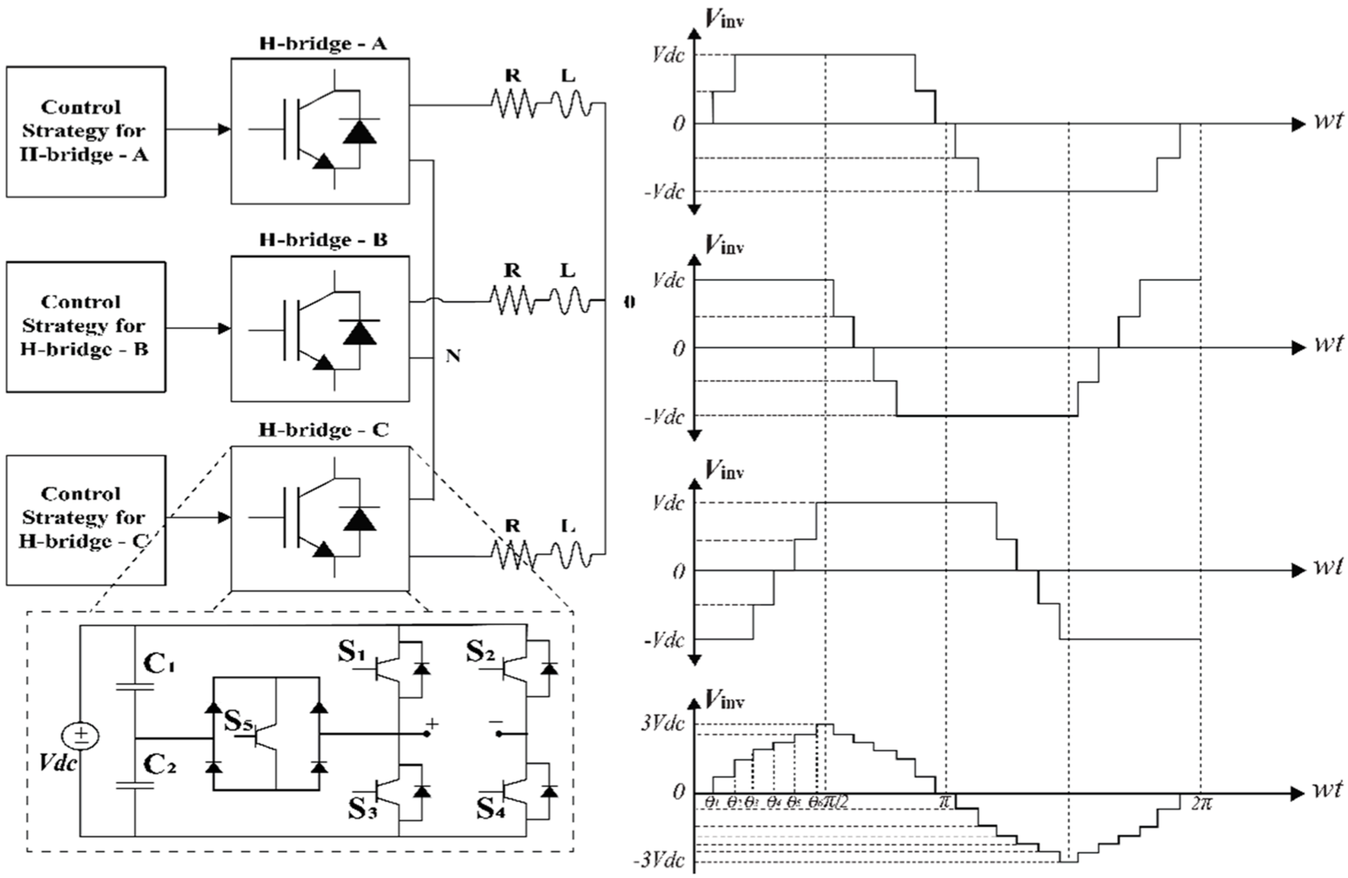

Fig. 2. Three-phase TCHB inverter block diagram with output voltage waveform.

Table 1
Switching state of a single unit of TCHB inverter.

No.	ON switches	Output Voltage level
1	S_1, S_4	$+ v_{dc}$
2	S_4, S_5	$+ 1/2v_{dc}$
3	S_1, S_2 Or $S_3,\ S_4$	0
4	S_2, S_5	$- 1/2v_{dc}$
5	S_2, S_3	$- v_{dc}$

signals by using comparators and logic gates, which are then sent to the appropriate switches [42]. Due to its simplicity, the NLC approach cannot successfully eliminate individual harmonics, making it unsuitable for systems with limited number of output levels [43].

The NLC approach was initially proposed by [16], and ensures that the output voltage closely approximates the reference voltage. The round function, often known as the nearest integer function, is designed to round numbers to the closest integer; for instance, round $\{1.6\} = 2$ and round $\{1.4\} = 1$. The nearest even number is used to round half-integers, so round $\{1.5\} = 2$. When comparing the reference voltage to the midpoint between two consecutive levels, the upper level is picked if it is at or above the midpoint, and the lower level if it is below the midway. The variable $v_{dc}/2$. sets a maximum approximation error. Fig. 3 illustrates the operational concept of the NLC method. To calculate the nearest voltage level, use the formula:

$$v = v_{dc} * round_{0.5}\ (v * /v_{dc}) \tag{2}$$

The NLC method for calculating switching angles at any number of

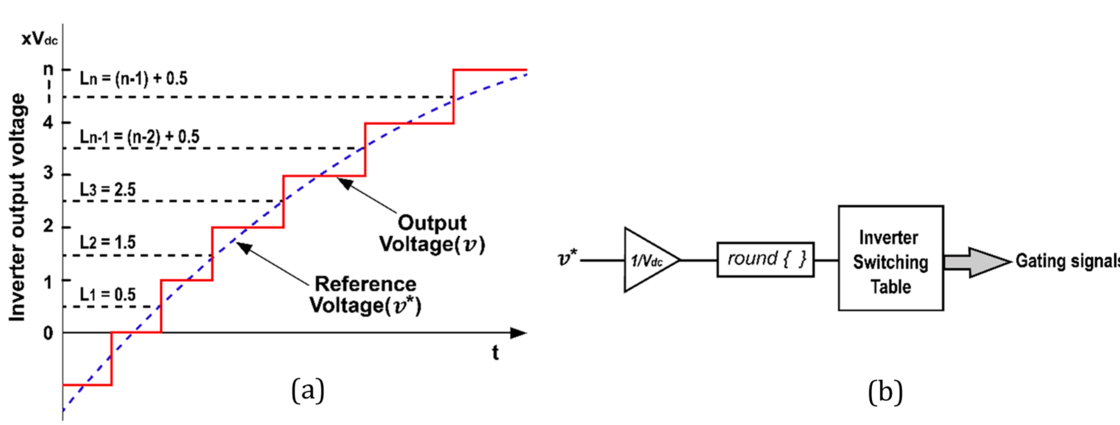

Fig. 3. Nearest level control technique (a) Level generation method (b) inverter switching logic.

layers is based on:

$$\theta_i = sin^{-1}\left(\frac{i-0.5}{x}\right) \tag{3}$$

Where $i = 1, 2, 3 \ldots \frac{n-1}{2}$, n is the number of levels and $x = \frac{n-1}{2}$

The waveform becomes almost sinusoidal as the number of levels increases when the θ_i get closer to one another, resulting in a waveform that is almost sinusoidal. The modulation index M for symmetrical TCHB MLIs can be determined using equation:

$$M = \frac{v_{ref}}{s \, * \, 0.5v_{dc}} \tag{4}$$

Where v_{ref} is the reference amplitude and s is denoting the steps number in a quarter wave .

2.3. Semiconductor losses and converter efficiency

The design and selection of converter circuits is significantly affected by semiconductor losses. These losses have a significant impact on the thermal management requirements, thus impacting on the total cost, volume, and weight of the inverter. The main types of semiconductor losses are static (conduction losses) and dynamic (switching losses). Conduction losses arise from the resistance experienced when the semiconductor devices are in the on-state, as well as the voltage drop that occurs in the forward direction.

The conduction losses of a transistor ($\sigma_{c,T}$) and a diode ($\sigma_{c,D}$) at a specific time (t) can be mathematically represented as:

$$\begin{cases} \sigma_{c,T}(t) = \left[v_T + R_T\ i^{\beta}(t)\right]i(t) \\ \sigma_{c,D}(t) = \left[v_D + R_D\ i(t)\right]i(t) \end{cases} \tag{5}$$

Where v_T and v_D represent the voltage drops that occur when the transistor and diode are in the on-state, while R_T and R_D represent their respective resistances in the on-state. The symbols β and $i(t)$ represent denote transistor amplification factor and instantaneous current through the transistor or diode, respectively.

The typical conduction losses for the transistor $P_{c,T}(t)$ and the diode $P_{c,D}(t)$ can be determined as:

$$\begin{cases} P_{c,T}(t) = \dfrac{1}{2\pi}\displaystyle\int_0^{2\pi}\left[\left\{v_T + R_T\ i^{\beta}(t)\right\}i(t)\right]d(\omega t) \\ P_{c,D}(t) = \dfrac{1}{2\pi}\displaystyle\int_0^{2\pi}\left[\left\{v_D + R_D\ i(t)\right\}i(t)\right]d(\omega t) \end{cases} \tag{6}$$

The contributions from each transistor and diode in the current path can then be added up to find the total average conduction losses $P_c(t)$, where $N_{Transitor}$ and N_{Diode} are the numbers of transistors and diodes, respectively:

$$P_c(t) = \int_0^{2\pi}\left[\left\{N_{Transitor}(t) * P_{c,T}(t)\right\} + \left\{N_{Diode}(t) * P_{c,D}(t)\right\}\right]d(\omega t) \tag{7}$$

Switching losses occur during the turn-on (t_{on}) and turn-off (t_{off}) periods of the semiconductor devices. The energy losses during turn-on (E_{on}) and turn-off (E_{off}) can be expressed as:

$$\begin{cases} E_{on} = \displaystyle\int_0^{t_{on}} v(t)\ i(t)dt = \int_0^{t_{on}}\left[\left(\frac{v_{sw}}{t_{on}} * t\right)\left(-\frac{I}{t_{on}}\right) * \ (t - t_{on})\right]dt = \frac{1}{6}v_{sw} * I * t_{on} \\ E_{off} = \displaystyle\int_0^{t_{off}} v(t)\ i(t)dt = \int_0^{t_{off}}\left[\left(\frac{v_{sw}}{t_{off}} * t\right)\left(-\frac{I'}{t_{off}}\right) * \ (t - t_{off})\right]dt = \frac{1}{6}v_{sw} * I' * t_{off} \end{cases} \tag{8}$$

Where v_{sw} and I represent the device's off-state voltage and current, respectively, and I' represents the device current measured immediately before it turns off. Calculation of total switching power losses (P_{sw}) over a given time period T is as follows:

$$P_{sw} = \frac{1}{T}\left[\sum_1^{N_{switch}}\left\{(N_{on} * E_{on}) + (N_{off} * E_{off})\right\}\right] \tag{9}$$

Where N_{on} and N_{off}, are the number of turn-on and turn-off events of a switch in a cycle.

Total semiconductor losses of this proposed TCHB MLI are the combined conduction and switching losses of all semiconductor devices employed, expressed as:

$$P_{total\_loss} = P_c(t) + P_{sw} \tag{10}$$

To determine the inverter efficiency (η), the output power P_{out} is used:

$$\eta\% = \left(\frac{P_{out}}{P_{total\_loss} + P_{out}}\right) * 100\% \tag{11}$$

The output power P_{out} can be calculated using:

$$P_{out} = \sqrt{3} * \frac{3v_{DC}}{\sqrt{2}} * \frac{I_{line}}{\sqrt{2}} * pf \tag{12}$$

Considering power factor (pf) of connected load is approximately 0.8 lagging, with a connected load, the resulting efficiency of the system is about 98 % using Eq. (13).

$$\eta(\%) = \left(\frac{P_{out}}{P_{in}}\right) * 100\% \tag{13}$$

3. PMSM modeling and control technique

The steady state and dynamic modelling of the PMSM from [44] are being expressed as:

$$v_d = R_s i_d + p\psi_d - \omega_r\psi_q \tag{14}$$

$$v_q = R_s i_d + p\psi_q - \omega_r\psi_d \tag{15}$$

$$\psi_d = L_d i_d + \psi_f \tag{16}$$

$$\psi_q = L_d i_d \tag{17}$$

$$\frac{di_d}{dt} = \frac{v_q - R_s i_d + \omega_r L_q i_q}{L_d} \tag{18}$$

$$\frac{di_q}{dt} = \frac{v_q - R_s i_q + \omega_r L_d i_d - \omega_r \psi_f}{L_q} \tag{19}$$

Eqs. (14) and (15) are transformed into Eqs. (18) and (19). The equation for the electromagnetic torque of PMSM is:

$$T_e = \frac{3}{2} n_p \left[\psi_f + (L_d - L_q) i_d\right] i_q \tag{20}$$

$$T_e = \frac{3}{2} n_p \psi_f i_q \tag{21}$$

In the above equations, the variable ψ_f represents the permanent magnet flux, $p = \frac{d}{dt}$ is the derivative operator, R_s indicates per phase stator resistance, rotor speed is ω_r, and n_p, L_s stands for no. of pole pairs and stator inductance respectively.

3.1. Control structure of the system

Fig. 4 shows the implementation of vector control, also known as field-oriented control, on a PMSM drive that is fed by a TCHB inverter. This control system comprises a dual closed-loop configuration, with one loop dedicated to current control and the other to speed control. Within a rotating coordinate system, the three-phase currents are transformed into the i_d and i_q components using the Clarke and Park transformations. The contrast between the q-axis current i_q and the reference current i_q^* derived from the speed loop is analyzed using a PI controller in the current loop. This output, combined with decoupling compensation, provides the reference voltage v_q^* for the q-axis.

The d-axis adopts control method employs a reference current of $i_d^* = 0$. These processes take place during normalization, where the reference voltage is restricted to ensure that the PMSM operates within the linear modulation range. Then, by using inverse Park transformation, reference voltages $v_d^*$and V_q^* in the rotating coordinate system are converted into $v_{ref\alpha}$ and $v_{ref\beta}$ components in the $\alpha\beta$ frame.

The components $v_{ref\alpha}$ and $v_{ref\beta}$ represent the instantaneous values of the reference voltages v_{ref}. The voltage vectors produced by the cascaded inverter are used to synthesize these reference voltages, which will then be modulated. At the end of the modulation algorithm is utilized to implement the switching sequence on cascaded inverter, resulting in simultaneous double closed-loop vector control of both current and speed.

The flow diagram illustrates in Fig. 5 shows the control structure of a closed-loop system for driving a PMSM using a TCHB inverter. First, the system receives a speed reference, which is compared to the motor's actual speed data from an encoder. The resulting error feeds into a PI controller, adjusting the i_q current reference. The i_q current is then compared with the sensed i_q value from the current sensor, with the error feeding into a secondary PI controller. For the i_d component, the system maintains a zero reference, and the difference between this and the sensed i_d current feeds into another PI controller to ensure optimal torque production.

Both current outputs from the PI controllers undergo transformations-first through an inverse Park (d-q to α-β) and then an inverse Clarke (α-β to a-b-c) transformation-generating voltage references. These references guide the NLC to create switching pulses for the TCHB inverter, which then powers the PMSM. The encoder and current sensors provide continuous feedback, ensuring the system dynamically adjusts for accurate tracking and minimized oscillations, reinforcing the closed-loop structure.

a. Park Transformation

The quantities in the two-axis orthogonal stationary reference frame are converted into rotating reference frame quantities through the Park transformation, as illustrated in Fig. 6(a). This transformation is represented by the following equations:

$$i_d = \ i_\alpha * \cos(\theta) + i_\beta * \sin(\theta) \tag{22}$$

$$i_q = i_\beta * \cos(\theta) - i_\alpha * \sin\,(\theta) \tag{23}$$

Where,

$i_d,\ i_q$ are rotating reference frame quantities
$i_\alpha,\ i_\beta$ are orthogonal stationary rotating reference frame quantities
ϴ is the rotation angel

b. Inverse Park Transformation

The quantities in the rotating reference frame are converted back to the two-axis orthogonal stationary reference frame using the Inverse

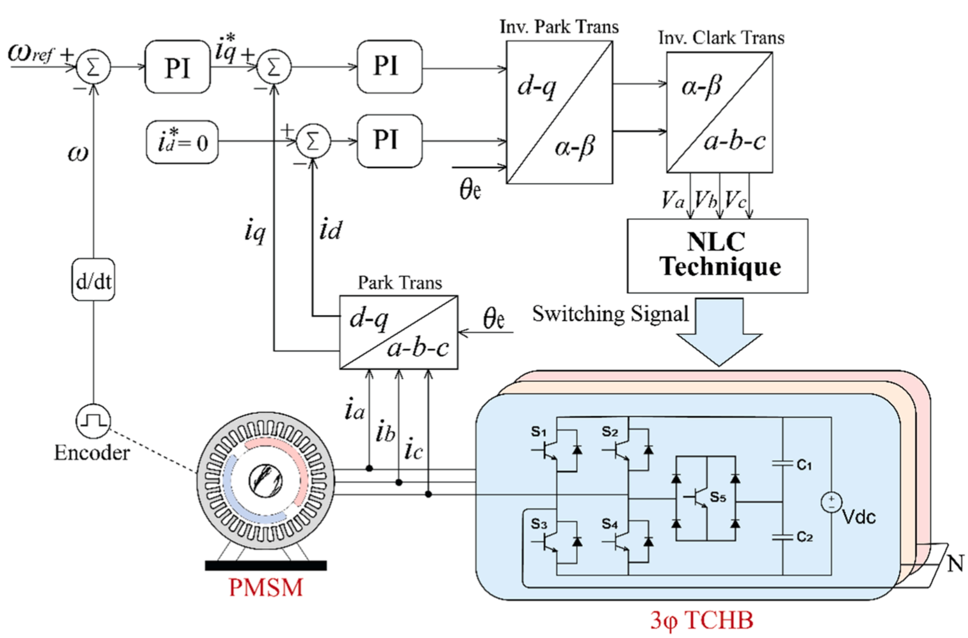

Fig. 4. Field Oriented Control Block Diagram of TCHB MLI fed PMSM System.

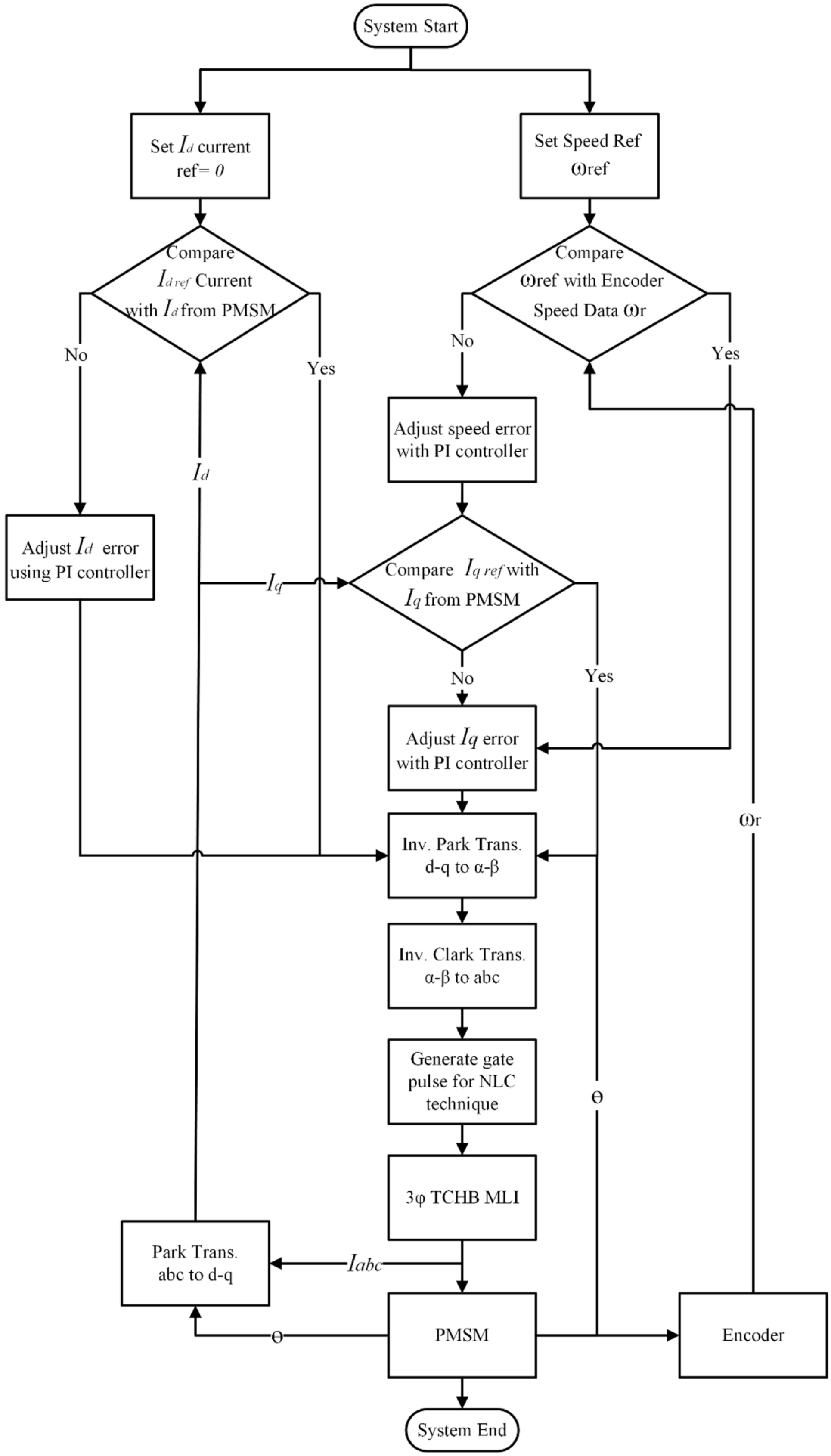

Fig. 5. Flow Chart of the Proposed FOC Controller.

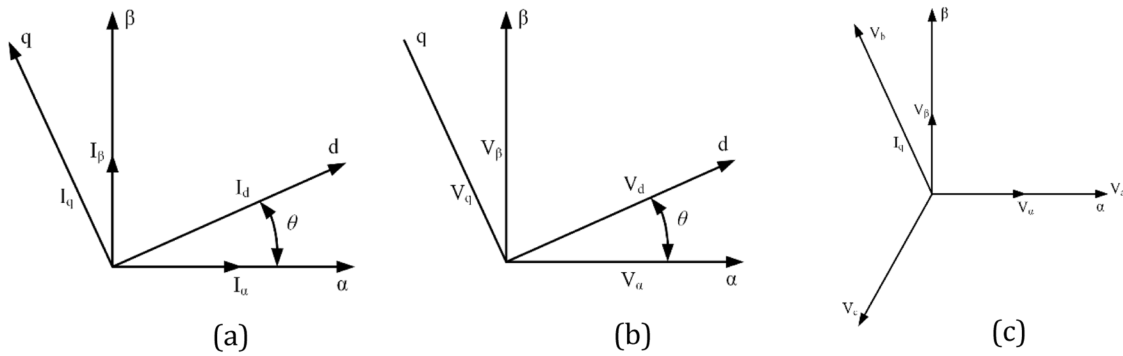

Fig. 6. Transformation vector diagram (a) Park transformation (b) Inverse Park transformation (c) Inverse Clarke transformation.

Park transformation, as illustrated in Fig. 6(b). This transformation is represented by the following equations:

$$v_\alpha = v_d * \cos(\theta) - v_q * \sin(\theta) \tag{24}$$

$$v_\beta = v_q * \cos(\theta) + v_d * \sin(\theta) \tag{25}$$

Where,

$v_\alpha,\ v_\beta$ are orthogonal stationary reference frame quantities
$v_d,\ v_q$ are rotating reference frame quantities
c. Inverse Clarke Transformation

The conversion from the two-axis orthogonal stationary reference frame to the three-phase stationary reference frame is achieved using the Inverse Clarke transformation, as illustrated in Fig. 6(c). This transformation is represented by the following equations:

$$v_a = v_\alpha \tag{26}$$

$$v_b = \frac{-v_\alpha + \sqrt{3} * v_\beta}{2} \tag{27}$$

$$v_c = \frac{-v_\alpha - \sqrt{3} * v_\beta}{2} \tag{28}$$

Where,

$v_a,\ v_b,\ v_c$ are three-phase quantities
$v_\alpha,\ v_\beta$ are stationary orthogonal reference frame quantities

4. Verification of inverter system using FOC strategies for PMSM

The MATLAB/Simulink software is used to simulate FOC. The NLC modulation technique is employed for generating the gate pulse for TCHB MLI. Table.2 shows the system parameters considered in simulation of closed loop system.

During the simulation of field-oriented control, two cases are taken into account: dynamic speed change with a constant reference torque, and dynamic torque change with a constant reference speed.

Table 2
Simulation Parameters Used for System Design.

	Parameter	Value
TCHB MLI	$v_{dc1}, v_{dc2}, v_{dc3}$	120 V
	Switching frequency	10 kHz
	Reference frequency	50 Hz
PMSM	Number of poles: P	3
	Rated Speed: N_s	2000 rpm
	Stator resistance: R_s	0.0918 Ω
	d-axis and q-axis inductance: L_d, L_q	0.975 mH
	Rated torque: T	20 Nm
	Magnet flux linkage: ψ_f	0.1688 Wb

4.1. Simulation with dynamic speed

The dynamic response of the PMSM drive fed by the TCHB inverter under closed-loop control using FOC during dynamic speed changes is depicted in Fig. 7(a)-(d). Fig. 7(a) illustrates the speed of the PMSM increasing from 300 rpm to 500 rpm at $t = 0.1\ s$, further increasing to 1000 rpm at $t = 0.2\ s$, then decreasing to 700 rpm at $t = 0.3\ s$, and subsequently rising to 1100 rpm and 1500 rpm at $t = 0.4\ s$ and $t = 0.5\ s$, respectively. The corresponding i_q response, torque response, and stator current of the system are depicted in Fig. 7(b), (c), and (d), respectively. The load torque is directly proportional to the electromagnetic torque and remains constant at 10 Nm. The q-axis current (i_q) and the electromagnetic torque (T_e) exhibit similar responses, with different magnitudes. During speed changes, the current waveforms in the stator winding experience a sudden increase in magnitude with a low frequency over a very brief period, as shown in Fig. 7(d). The torque also changes and quickly returns to its reference value.

Fig. 7(a) clearly illustrates that the TCHB inverter-fed PMSM drive accurately tracks the reference speed changes (both of increasing as well as decreasing) without any noticeable oscillations. Additionally, Fig. 7 (d) depicts that the stator current remains consistent during variations in reference speed.

4.2. Simulation with dynamic torque

The dynamic response under closed-loop control using FOC during dynamic torque changes is shown in Figs. 8(a)-(d) for the PMSM drive fed by the TCHB inverter. Fig. 8(a) shows the torque of the PMSM decreasing from 10 Nm to 20 Nm at $t = 0.1\ s$, increasing to 30 Nm at $t = 0.2\ s$, decreasing again to 10 Nm at $t = 0.3\ s$, and then increasing to 15 Nm and 40 Nm at $t = 0.4\ s$ and $t = 0.5\ s$, respectively. The corresponding speed response, i_q response, and stator current are depicted in Fig. 8(b), (c), and (d), accordingly. The reference speed, which stays constant at 1000 rpm, is closely followed by the actual speed. Fig. 8(d) demonstrates that the stator current adjusts according to the torque changes to maintain constant speed.

Fig. 9 illustrates the effectiveness of the NLC modulation technique in minimizing THD, achieving a current THD of 4.73 %. This reduction in harmonic distortion signifies a substantial enhancement in the waveform quality of the TCHB MLI-fed PMSM drive, making it highly suitable for electric vehicle applications where minimal power losses and high-quality output are essential. The NLC technique's advantage lies in its ability to reduce switching losses and optimize inverter efficiency. Though the NLC technique is effective in reducing switching losses and improving inverter efficiency, it faces several limitations. Voltage balancing issues may also occur, as imbalances across the DC sources or capacitors can lead to incorrect switching and reduced performance. The NLC method performs best under stable operating

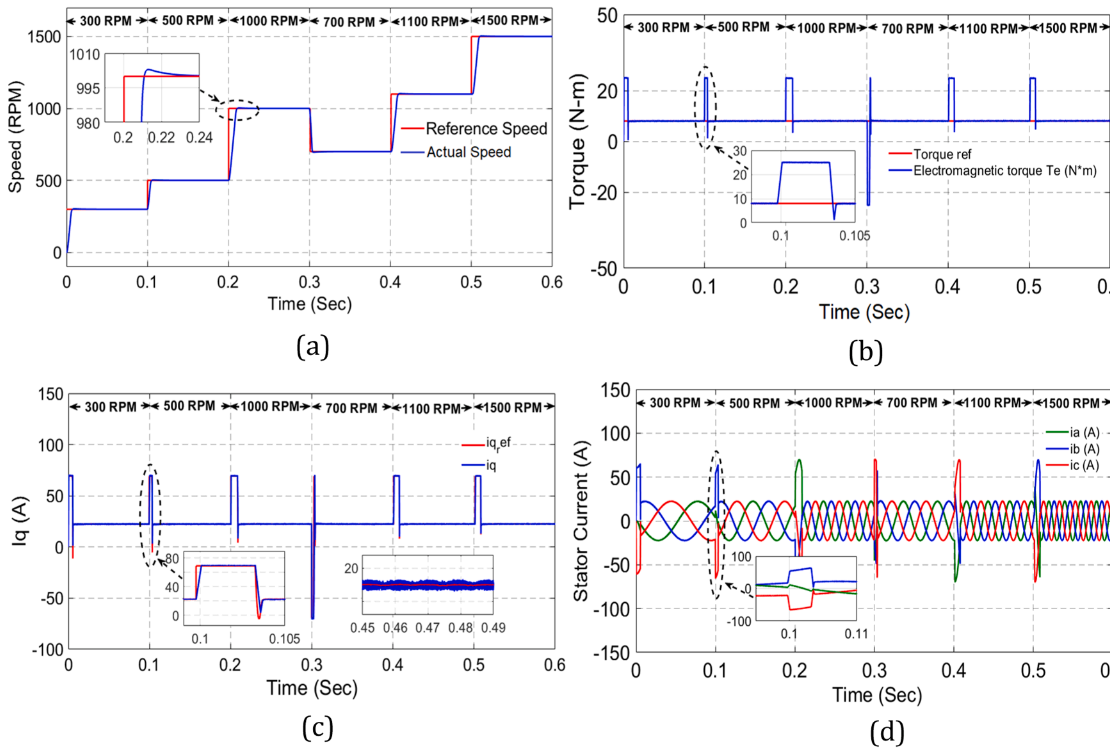

Fig. 7. Waveform of the TCHB inverter fed PMSM drive system with variable speed (a) Speed (b) Torque (c) I_q current and (d) Stator current.

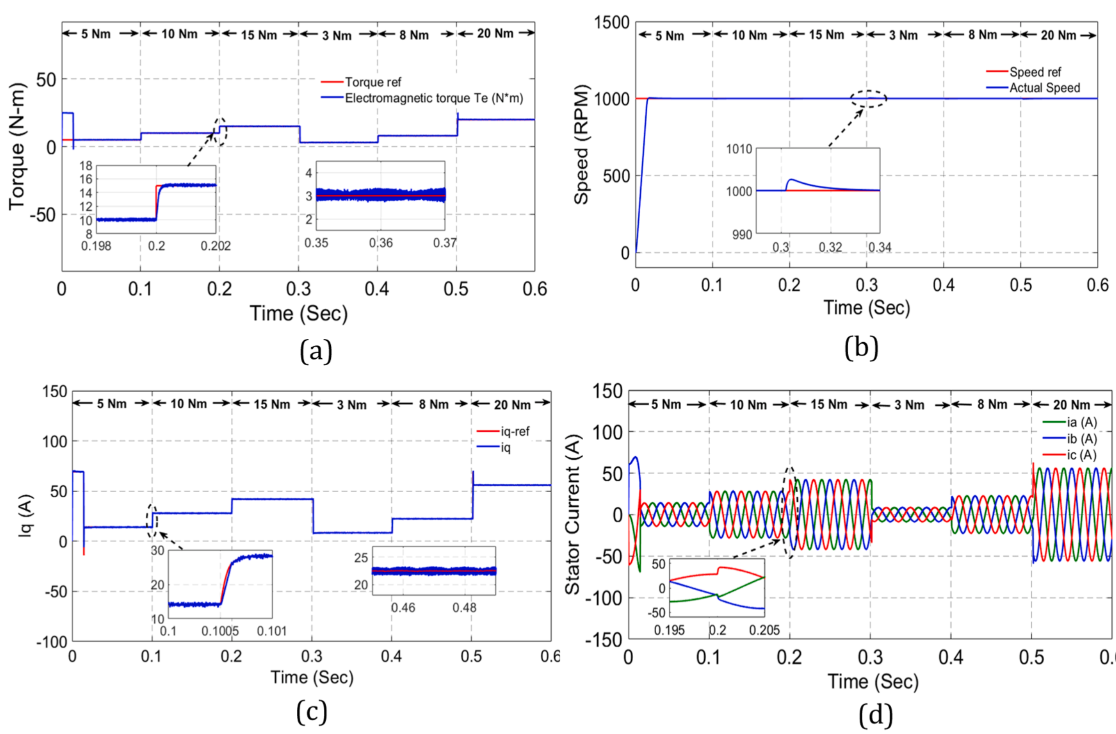

Fig. 8. Waveform of the TCHB inverter fed PMSM drive system with variable torque (a) Torque (b) Speed (c) I_q current and (d) Stator current.

conditions, and dynamic changes in load or input voltage can introduce quantization errors, resulting in higher THD. Overcoming these limitations will be essential for optimizing the technique in practical hardware applications.

The performance of the TCHB inverter-fed PMSM system is further demonstrated in Fig. 10, where efficiency metrics are presented across different operating speeds. The results indicate that the system's efficiency is notably higher in the high-speed region, primarily due to reduced core losses and improved inverter performance. This trend reflects the system's suitability for high-speed applications, such as electric vehicle drives, where maintaining efficiency at various speeds is crucial. However, ensuring consistent efficiency under load variations

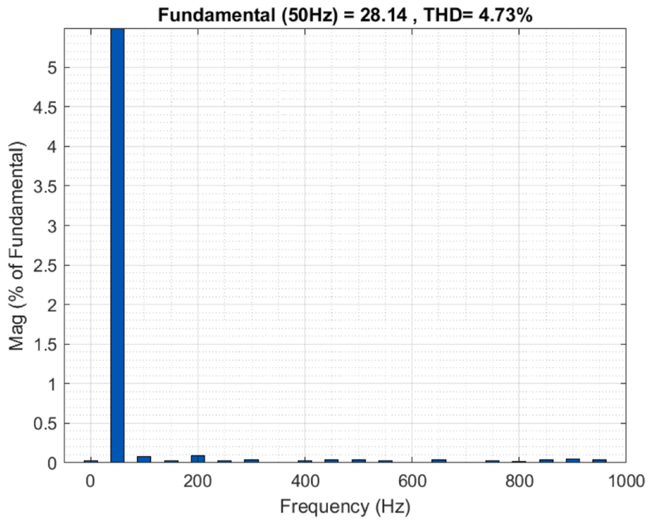

Fig. 9. Harmonic spectrum of the phase current.

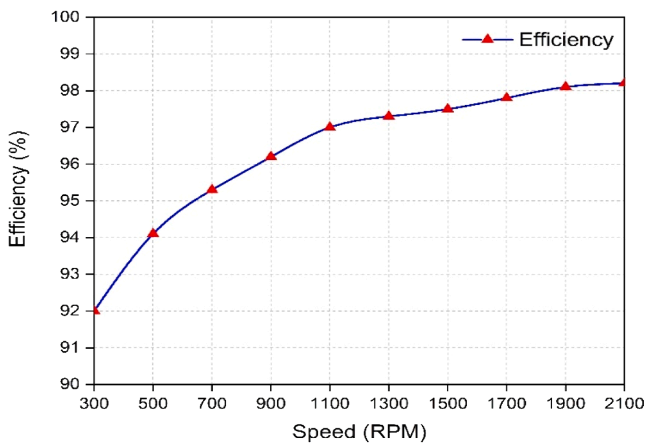

Fig. 10. Overall efficiency of the TCHB inverter fed PMSM system.

will be vital for real-world implementation, especially when considering practical applications in renewable energy or EV systems.

To assess the real-world applicability of the proposed inverter system for EVs, an urban drive cycle was employed to evaluate its performance. Fig. 11 illustrates the drive cycle trajectory and the system's precise tracking of the reference, demonstrating the inverter's ability to respond dynamically to the fluctuating demands of an urban driving environment. This result underscores the system's suitability for real-world EV applications, validating its capacity for accurate speed and torque tracking, as required for efficient and reliable EV operation.

4.3. Comparison with relevant literature studies

This research assesses the performance of the proposed NLC method implemented in a three-phase TCHB inverter compared to other methods existing in the literature. The comparison focuses on two main performance metrics, THD and the number of levels generated to demonstrate how the NLC method enhances system efficiency and power quality.

Several studies have investigated alternative modulation strategies for TCHB inverters, such as SHE. While SHE is effective at selectively removing harmonics, its performance deteriorates outside a narrow modulation index, leading to a higher THD. In [45], a 13-level symmetrical TCHB inverter using SHE method achieved a THD of around 6.77 %. In contrast, this research shows that the NLC-based approach lowers THD to 4. 7 %, even across a broader range of operation, indicating superior harmonic performance and more consistent power quality.

Other studies [8] also explore techniques like Carrier Based Pulse Width Modulation (CBPWM) and Space Vector Pulse Width Modulation (SVPWM), where author shows how SVPWM reduced THD compare to CBPWM around 13.12 % from 29.17 % voltage THD for same switching frequency, though it based on 5-level output. Another study using Phase-shift Pulse Width Modulation (PDPWM) for three-phase TCHB MLI uses total of 30 switches to generate 9-level output, achieves voltage THD of 9.30 % [46]. The NLC method, however, operates at lower switching frequencies, which not only helps maintain the better THD but also significantly reduces switching losses, making it a more efficient solution in high-power applications.

When comparing control strategies, this research incorporates FOC for the PMSM drive. Other control techniques, like Direct Torque Control (DTC) and scalar control, while popular, are less precise. DTC, for instance, often results in higher torque ripples and less smooth operation [47]. A comparative study shows that Model Predictive Current Control (MPCC) for PMSM has larger current ripple than FOC, and FOC has batter performance based on dynamic conditions [48].

In contrast, FOC provides highly accurate motor control, ensuring smooth reference speed tracking without significant oscillations.

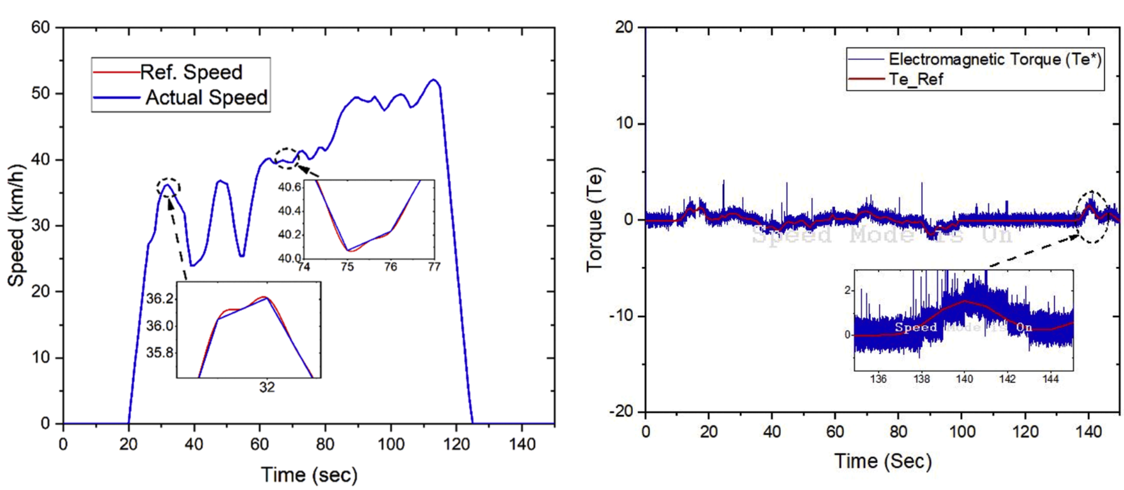

(a) (b)

Fig. 11. Performance evaluation (a) Drive cycle trajectory and (b) The system's tracking.

Table 3
Summary of recent modulation technique applied to TCHB MLI.

Modulation Technique	Inverter Type	THD (%)	Observations
SHE [45]	13-Level TCHB	6.77 %	Effective in narrow range but THD increases outside narrow modulation range
CBPWM [8]	5-Level TCHB	29.17 %	Higher THD compared to SVPWM, which offers better performance
SVPWM [8]	5-Level TCHB	13.12 %	Improved THD reduction over CBPWM
PDPWM [46]	9-Level TCHB	9.3 %	Achieved with 30 switches; moderately high THD
Model Predictive Control (MPC) [49]	13-Level TCHB	10.22 %	Though it uses 15 switches for 13-level, it still has high voltage THD.
ANN based Modulation [50]	5-Level TCHB	14.48 %	ANN technique provides lower THD content at output compared with PSO technique, but higher than NLC
NLC (Proposed Method)	13-Level TCHB	4.73 %	NLC maintains low THD across a wide modulation range, superior harmonic performance.

Table 4
Summary of control techniques applied to PMSM motor drive.

Control Technique	Motor Type	Results	Observation
MPCC [47]	PMSM	Higher current ripple	Greater ripple compared to FOC, less precise
DTC [48]	PMSM	Higher torque ripple	Less smooth operation, especially under dynamic conditions
FOC [29]	PMSM	Accurate, stable	Ensures smooth reference tracking and stable torque without ripples

Additionally, torque variations are managed effectively to maintain stable speed [29], which highlights the combined strength of the FOC and NLC methods in providing dynamic and steady-state performance.

Tables 3 and 4 summarizes the benefits of NLC and FOC integration in achieving superior performance in THD reduction, efficient power quality, and precise motor control, especially for high-efficiency applications.

Overall, this comparison demonstrates that the NLC-based TCHB inverter, paired with FOC, surpasses other controllers and modulation techniques in minimizing THD, reducing switching losses, and delivering precise motor control. This system is particularly suitable for applications requiring high power efficiency and superior performance, such as in EV and renewable energy systems. Future research should aim at experimentally validating these findings and exploring additional advanced control strategies to further enhance system performance.

5. Conclusions

This research demonstrates the effectiveness of the NLC technique in a three-phase TCHB multilevel inverter designed for EV operations. The NLC method achieves a notable reduction in THD, achieving a THD of 4.73 % under stable operating conditions, which is significantly lower than typical values in conventional systems without NLC. Additionally, the application of NLC results in an overall system efficiency improvement, achieving over 97 % efficiency at optimal speed and torque conditions, contributing to enhanced power quality and reduced energy losses. Simulation results confirm that the TCHB inverter, coupled with the NLC technique, delivers excellent performance in handling dynamic speed and torque variations in PMSM drives. The system demonstrated smooth reference speed tracking with a response time of <0.04 s, showing minimal oscillations and efficiently adjusting to torque variations to maintain consistent speed. This capability indicates the system's potential for dynamic adaptability required in EV applications. Furthermore, the integration of FOC provides precise control of the PMSM, minimizing torque ripples and ensuring superior dynamic and steady-state performance. Despite the promising results, the system's performance under extreme operating conditions, such as high-speed or high-torque scenarios remain unexplored. Future research should focus on investigating other control strategies, including MPC or machine learning based control to enhance adaptability and efficiency of the overall system. Moreover, extending the study to examine the impact of power quality in grid-connected applications and exploring the integration of renewable energy sources could open new potential application of the TCHB inverter.

CRediT authorship contribution statement

Md Showkot Hossain: Writing – review & editing, Writing – original draft, Software, Methodology, Data curation, Conceptualization. **Nurul Ain Mohd Said:** Writing – review & editing, Supervision. **Md Akib Hasan:** Writing – review & editing, Software, Formal analysis. **Wahidah Abd Halim:** Visualization, Validation, Supervision, Methodology. **Wan Noraishah Wan Abdul Munim:** Investigation, Formal analysis. **Auzani Jidin:** Supervision, Software, Methodology, Conceptualization.

Declaration of competing interest

The authors declare that they have no known competing financial interests or personal relationships that could have appeared to influence the work reported in this paper.

Acknowledgments

This research was funded by the Center of Research and Innovation Management (CRiM) and Faculty of Electrical Technology and Engineering, Universiti Teknikal Malaysia Melaka.

Declaration of generative AI and AI-assisted technologies in the writing process

During the modification of article author Md Showkot Hossain used ChatGPT in order to check the speling, grammar and improve the writing. After using the tool, the author reviewed and edited the content as required and take full responsibility.

Data availability

Data will be made available on request.

References

[1] M.M. Hasan, A. Abu-Siada, M.S.A. Dahidah, A three-phase symmetrical DC-link multilevel inverter with reduced number of DC sources, IEEE Trans. Power Electron. 33 (10) (2018) 8331–8340, https://doi.org/10.1109/TPEL.2017.2780849.

[2] M. Chen, Y. Yang, X. Liu, P.C. Loh, F. Blaabjerg, Single-source cascaded multilevel inverter with voltage-boost submodule and continuous input current for photovoltaic applications, IEEE Trans. Power Electron. 37 (1) (Jan. 2022) 955–970, https://doi.org/10.1109/TPEL.2021.3098015.

[3] S. Xu, Z. Sun, C. Yao, H. Zhang, W. Hua, G. Ma, Model predictive control with constant switching frequency for three-level T-type inverter-fed PMSM drives, IEEE Trans. Ind. Electron. 69 (9) (Sep. 2022) 8839–8850, https://doi.org/10.1109/TIE.2021.3114716.

[4] M. Vijeh, M. Rezanejad, E. Samadaei, K. Bertilsson, A general review of multilevel inverters based on main submodules: structural point of view, IEEE Trans. Power Electron. 34 (10) (2019) 9479–9502, https://doi.org/10.1109/TPEL.2018.2890649.

[5] M.S. Hossain, N.A.M. Said, W.Abd Halim, M.H. Hossain, Comparing performance and complexity of TCHB and CHB multilevel inverters using NLC technique, Int. J. Power Electron. Drive Syst. 15 (1) (2024) 292–302, https://doi.org/10.11591/ijpeds.v15.i1.pp292-302.

[6] I. Saady, M. Karim, B. Bossoufi, N. El Ouanjli, S. Motahhir, B. Majout, Optimization and control of photovoltaic water pumping system using kalman filter based MPPT

and multilevel inverter fed DTC-IM, Results Eng. 17 (2023) 100829, https://doi.org/10.1016/j.rineng.2022.100829.

[7] M.S. Hossain, M.I. Hossain, N.A.M. Said, W.A. Halim, S.N.M. Azam, M.H. Hossain, Nearest level control technique for three-phase transistor clamped H-bridge multilevel inverter, in: 2022 IEEE Int. Conf. Power Energy, 2022, pp. 71–76, https://doi.org/10.1109/PECON54459.2022.9988919.

[8] P. Jayal, G. Bhuvaneswari, A novel space vector modulation-based transistor-clamped H bridge inverter-fed permanent magnet synchronous motor drive for electric vehicle applications, Int. Trans. Electr. Energy Syst. (2021). Wiley Online Libr., Accessed: Mar. 21, 2023. [Online]. Available: https://onlinelibrary.wiley.com/doi/abs/10.1002/2050-7038.12789.

[9] A.V. Khergade, R.J. Satputaley, V.B. Borghate, B.V.S. Raghava, Harmonics reduction of adjustable speed drive using transistor clamped H-bridge inverter based DVR with enhanced capacitor voltage balancing, IEEE Trans. Ind. Appl. 56 (6) (2020) 6744–6755, https://doi.org/10.1109/TIA.2020.3013823.

[10] M.F.M. Elias, N.A. Rahim, H.W. Ping, M.N. Uddin, Asymmetrical cascaded multilevel inverter based on transistor-clamped H-bridge power cell, IEEE Trans. Ind. Appl. 50 (6) (2014) 4281–4288, https://doi.org/10.1109/TIA.2014.2346711.

[11] K.K. Gupta, A. Ranjan, P. Bhatnagar, L.K. Sahu, Multilevel inverter topologies with reduced device count: a review, IEEE Trans. Power Electron. (2015) ieeexplore.ieee.org, Accessed: Mar. 21, 2023. [Online]. Available: https://ieeexplore.ieee.org/abstract/document/7050287/.

[12] A. Salem, H. Van Khang, K.G. Robbersmyr, M. Norambuena, J. Rodriguez, Voltage source multilevel inverters with reduced device count: topological review and novel comparative factors, IEEE Trans. Power Electron. 36 (3) (2021) 2720–2747, https://doi.org/10.1109/TPEL.2020.3011908.

[13] E. Bushra, K. Zeb, I. Ahmad, M. Khalid, A comprehensive review on recent trends and future prospects of PWM techniques for harmonic suppression in renewable energies based power converters, Results Eng. 22 (2024) 102213, https://doi.org/10.1016/j.rineng.2024.102213.

[14] O. Zolfagharian, A. Dastfan, Robust multicarrier modulation technique for multilevel inverters against unequal DC voltages, IEEE J. Emerg. Sel. Top. Power Electron. 12 (3) (2024) 3005–3017, https://doi.org/10.1109/JESTPE.2024.3373688.

[15] M. Soltani, M.H. Khanzadeh, Comparison of switching methods for asymmetric cascaded h- bridge multilevel inverter, IOSR J. Eng 05 (08) (2015) 52–60. https://www.iosrjen.org/Papers/vol5_issue8%20(part-3)/H05835260.pdf.

[16] S. Kouro, R. Bernal, H. Miranda, C.A. Silva, J. Rodriguez, High-performance torque and flux control for multilevel inverter fed induction motors, IEEE Trans. Power Electron. 22 (6) (2007) 2116–2123, https://doi.org/10.1109/TPEL.2007.909189.

[17] M.F.M. Elias, N.A. Rahim, H.W. Ping, M.N. Uddin, Asymmetrical cascaded multilevel inverter based on transistor-clamped H-bridge power cell, IEEE Trans. Ind. Appl. 50 (6) (2014) 4281–4288, https://doi.org/10.1109/TIA.2014.2346711.

[18] G.T. Son, et al., Design and control of a modular multilevel HVDC converter with redundant power modules for noninterruptible energy transfer, IEEE Trans. Power Deliv. 27 (3) (2012) 1611–1619, https://doi.org/10.1109/TPWRD.2012.2190530.

[19] R.B. Jonnala, N.R. Eluri, S.B. Choppavarapu, Implementation, comparison and experimental verification of nearest vector control and nearest level control techniques for 27-level asymmetrical CHB multilevel inverter, in: 2016 Int. Conf. Control Instrum. Commun. Comput. Technol. ICCICCT 2016, 2017, pp. 214–221, https://doi.org/10.1109/ICCICCT.2016.7987947.

[20] H.T. Khamees, A.S. Hussein, N.I. Abdulkhaleq, An evaluation of scintillation index in atmospheric turbulent for new super Lorentz vortex Gaussian beam, Telkomnika (Telecommunication Comput. Electron. Control. 21 (1) (2023) 1–7, https://doi.org/10.12928/TELKOMNIKA.v21i1.22221.

[21] H. Khamees, H. Salloom, I. Akram, Near-field propagation of a flat-topped gaussian beam: analysis in weakly turbulent atmospheres, Edelweiss Appl. Sci. Technol. 8 (2024) 1426–1433, https://doi.org/10.55214/25768484.v8i5.1845.

[22] D. Woldegiorgis, H.A. Mantooth, Precise electro-thermal power loss model of a three-level ANPC inverter with hybrid Si/SiC switches, Chinese J. Electr. Eng. 8 (3) (2022) 76–89, https://doi.org/10.23919/CJEE.2022.000027.

[23] R. S, J. R, Review on electric mobility: trends, challenges and opportunities, Results Eng. 23 (2024) 102631, https://doi.org/10.1016/j.rineng.2024.102631.

[24] A. Kersten, O. Theliander, E.A. Grunditz, T. Thiringer, M. Bongiorno, Battery loss and stress mitigation in a cascaded H-bridge multilevel inverter for vehicle traction applications by filter capacitors, IEEE Trans. Transp. Electrif. 5 (3) (2019) 659–671, https://doi.org/10.1109/TTE.2019.2921852.

[25] A. Kasri, K. Ouari, Y. Belkhier, A. Oubelaid, M. Bajaj, M. Berhanu Tuka, Real-time and hardware in the loop validation of electric vehicle performance: robust nonlinear predictive speed and currents control based on space vector modulation for PMSM, Results Eng. 22 (2024) 102223, https://doi.org/10.1016/j.rineng.2024.102223.

[26] X. Chi, et al., A ripple suppression of sensorless FOC of PMSM electrical drive system based on MRAS, Results Eng. 20 (2023) 101427, https://doi.org/10.1016/j.rineng.2023.101427.

[27] H. Ghanayem, M. Alathamneh, R.M. Nelms, Three-phase PMSM vector control using decoupled flux and speed controller, Energy Rep. 9 (2023) 645–652, https://doi.org/10.1016/j.egyr.2023.03.090.

[28] H. Djouadi, K. Ouari, Y. Belkhier, H. Lehouche, M. Bajaj, V. Blazek, Improved robust model predictive control for PMSM using backstepping control and incorporating integral action with experimental validation, Results Eng. 23 (2024) 102416, https://doi.org/10.1016/j.rineng.2024.102416.

[29] K. Mathew K, D.M. Abraham, A. Harish, Speed regulation of PMSM drive in electric vehicle applications with sliding mode controller based on harris Hawks optimization, e-Prime - Adv. Electr. Eng. Electron. Energy 9 (2024) 100643, https://doi.org/10.1016/j.prime.2024.100643.

[30] T. Song, Z. Zhang, H. Liu, W.L. Hu, Multi-objective optimisation design and performance comparison of permanent magnet synchronous motor for EVs based on FEA, IET Electr. Power Appl. 13 (8) (2019) 1157–1166, https://doi.org/10.1049/iet-epa.2019.0069.

[31] P. Ramesh, M. Umavathi, C. Bharatiraja, G. Ramanathan, S. Athikkal, Development of a PMSM motor field-oriented control algorithm for electrical vehicles, Mater. Today Proc. 65 (2022) 176–187, https://doi.org/10.1016/j.matpr.2022.06.080.

[32] T. Odabaşı, A. Tap, L.T. Ergene, Simulation and design of a sensorless FOC driver for a PMSM used in compressor, in: 2021 3rd Global Power, Energy and Communication Conference (GPECOM), 2021, pp. 97–102, https://doi.org/10.1109/GPECOM52585.2021.9587521.

[33] M. Megrini, A. Gaga, Y. Mehdaoui, J. Khyat, Design and PIL test of extended Kalman filter for PMSM field oriented control, Results Eng. 24 (2024) 102843, https://doi.org/10.1016/j.rineng.2024.102843.

[34] F. Yang, Z. Ming, T. Wen, T. Zhang, Z. Zhu, Research on control methods of permanent magnet synchronous motor position servo system, in: 2015 International Conference on Advanced Mechatronic Systems (ICAMechS), 2015, pp. 261–266, https://doi.org/10.1109/ICAMechS.2015.7287070.

[35] A.R. Kumar, D. Thangavelusamy, RETRACTED: a modified nearest level modulation scheme for symmetric and asymmetric configurations of cascaded H-bridge inverter, Int. J. Electr. Eng. \& Educ. 60 (1_suppl) (2023) 1341–1356, https://doi.org/10.1177/0020720919858844.

[36] H. Yao, Y. Yan, T. Shi, G. Zhang, Z. Wang, C. Xia, A novel SVPWM scheme for field-oriented vector-controlled PMSM drive system fed by cascaded H-bridge inverter, IEEE Trans. Power Electron. 36 (8) (2021) 8988–9000, https://doi.org/10.1109/TPEL.2021.3054642.

[37] J. Jacob, A. Chitra, Field oriented control of space vector modulated multilevel inverter fed PMSM drive, Energy Procedia 117 (2017) 966–973, https://doi.org/10.1016/j.egypro.2017.05.217.

[38] M.K.B. Boumegouas, K. Kouzi, A new synergetic scheme control of electric vehicle propelled by six-phase permanent magnet synchronous motor, Adv. Electr. Electron. Eng. 20 (1) (2022) 1–14, https://doi.org/10.15598/aeee.v20i1.4221.

[39] M. Hasoun, A. El Afia, M. Khafallah, K. Benkirane, Field oriented control based on a 24-sector vector space decomposition for dual three-phase pmsm applied on electric ship propulsion, Int. J. Power Electron. Drive Syst. 11 (3) (2020) 1175–1187, https://doi.org/10.11591/ijpeds.v11.i3.pp1175-1187.

[40] G.T. Son, et al., Design and control of a modular multilevel HVDC converter with redundant power modules for noninterruptible energy transfer, IEEE Trans. Power Deliv. 27 (3) (2012) 1611–1619, https://doi.org/10.1109/TPWRD.2012.2190530.

[41] H. Rashid, et al., A comprehensive review on economic, environmental impacts and future challenges for photovoltaic-based electric vehicle charging infrastructures, Front. Energy Res. 12 (2024), https://doi.org/10.3389/fenrg.2024.1411440.

[42] Q. Tu, Z. Xu, Impact of sampling frequency on harmonic distortion for modular multilevel converter, IEEE Trans. Power Deliv. 26 (1) (2011) 298–306, https://doi.org/10.1109/TPWRD.2010.2078837.

[43] R. José, et al., Multilevel converters: an enabling technology for high-poer applications, Proc. IEEE 97 (11) (2009) 1786–1817, https://doi.org/10.1109/JPROC.2009.2030235.

[44] O. Benjak, D. Gerling, Review of position estimation methods for IPMSM drives without a position sensor part II: adaptive methods, in: The XIX International Conference on Electrical Machines - ICEM 2010, 2010, pp. 1–6, https://doi.org/10.1109/ICELMACH.2010.5607980.

[45] W.A. Halim, N.A. Rahim, M. Azri, Selective harmonic elimination for a single-phase 13-level TCHB based cascaded multilevel inverter using FPGA, J. Power Electron. 14 (3) (2014) 488–498, https://doi.org/10.6113/JPE.2014.14.3.488.

[46] S. Vinnakoti and V.R. Kota, "Performance evaluation of TCHB multilevel inverter with level-shifted PWM scheme," no. November, pp. 47–59, 2015, doi: 10.3850/978-981-09-5247-1_006.

[47] N. Li, Y. Ming, G. Xianguo, X. Dianguo, A comparative study of model predictive current control and FOC for PMSM, in: 2014 17th International Conference on Electrical Machines and Systems (ICEMS), 2014, pp. 3143–3147, https://doi.org/10.1109/ICEMS.2014.7014034.

[48] F. Korkmaz, İ. Topaloğlu, M.F. Çakir, R. Gürbüz, Comparative performance evaluation of FOC and DTC controlled PMSM drives, in: 4th International Conference on Power Engineering, Energy and Electrical Drives, 2013, pp. 705–708, https://doi.org/10.1109/PowerEng.2013.6635696.

[49] K. Rameshkumar, V. Indragandhi, G. Mani, P. Sanjeevikumar, Model predictive current control of single-phase 13-level transistor-clamped H-bridge based cascaded multilevel inverter, in: Lecture Notes in Electrical Engineering, 436, Springer Verlag, 2017, pp. 597–608, https://doi.org/10.1007/978-981-10-4394-9_58.

[50] M. Rasheed, M.M.A. Alakkad, R. Omar, M. Sulaiman, W.A. Halim, Enhance the accuracy of control algorithm for multilevel inverter based on artificial neural network, Indones. J. Electr. Eng. Comput. Sci. 20 (3) (2020) 1148–1158, https://doi.org/10.11591/ijeecs.v20.i3.pp1148-1158.